

Correcting Crown-Level Clumping Effect for Improving Leaf Area Index Retrieval From Large-Footprint LiDAR: A Study Based on the Simulated Waveform and GLAS Data

Hailan Jiang¹, Guangjian Yan, *Senior Member, IEEE*, Yiyi Tong², Shiyu Cheng, Xuebo Yang³, Ronghai Hu⁴, Linyuan Li⁵, *Associate Member, IEEE*, Xihan Mu⁶, Donghui Xie⁷, Wuming Zhang, Guoqing Zhou⁸, and Felix Morsdorf⁹

Abstract—The demand for leaf area index (LAI) retrieval from spaceborne full-waveform LiDAR increases due to its direct sampling of the three-dimensional forest structure at a near-global scale. However, the nonrandomness (i.e., clumping effect) of canopy composition limits the reliability of LAI derived from two common methods. They either assume a homogeneous scene in the footprint or just correct for the large gaps-induced between-crown clumping. The clumping in the crown is still an unaddressed issue. We proposed a method to compensate occlusion (i.e., lower canopy layers are occluded by the upper canopy in the process of LiDAR measurement), through which the vertical canopy profile can be resolved from the waveform. Further, we developed a method

of deriving relative path length distribution that can reflect the heterogeneity of the canopy from the occlusion-corrected waveform. In addition to correcting the between-crown clumping, we corrected the within-crown clumping further using the derived relative path length distribution, based on path length distribution (PATH) theory. We used simulated waveform data with known LAI and GLAS data with corresponding field-measured LAI to test the performance of our and the other two common LAI retrieval methods. Results show that the errors of our approach are the lowest (with an error generally below 10% and the maximum error below 20%, compared with up to 69% and 47% for the other two methods), and it is relatively stable in various scenes. This study demonstrated the potential of improving LAI retrieval through full utilization of full-waveform data.

Manuscript received July 6, 2021; revised October 2, 2021; accepted November 12, 2021. Date of publication November 25, 2021; date of current version December 15, 2021. This work was supported in part by the Key Program of the National Natural Science Foundation of China (NSFC) under Grant 42090013 and Grant 41971380, in part by the Guangxi Natural Science Fund for Innovation Research Team under Grant 2019GXNSFGA245001, in part by the University of Zurich Research Priority Program on Global Change and Biodiversity (URPP GCB), and in part by the China Scholarship Council. (*Corresponding author: Guangjian Yan.*)

Hailan Jiang is with the State Key Laboratory of Remote Sensing Science, Faculty of Geographical Science, Beijing Normal University, Beijing 100875, China, and also with the Remote Sensing Laboratories Department of Geography, University of Zurich, CH-8057 Zurich, Switzerland. (e-mail: jianghailansea@163.com).

Guangjian Yan, Yiyi Tong, Shiyu Cheng, Linyuan Li, Xihan Mu, and Donghui Xie are with the State Key Laboratory of Remote Sensing Science, Faculty of Geographical Science, Beijing Normal University, Beijing 100875, China (e-mail: gjyan@bnu.edu.cn; tongyiyi0311@163.com; 201821051064@mail.bnu.edu.cn; lilinyuan@bjfu.edu.cn; muxihan@bnu.edu.cn; xiedonghui@bnu.edu.cn).

Xuebo Yang is with the Key Laboratory of Digital Earth Science, Aerospace Information Research Institute Chinese Academy of Sciences, Beijing 100094, China (e-mail: yangxb@radi.ac.cn).

Ronghai Hu is with the College of Resources and Environment, University of Chinese Academy of Sciences, Beijing 100049, China (e-mail: huronghai@ucas.ac.cn).

Wuming Zhang is with the School of Geospatial Engineering and Science, Sun Yat-sen University, Zhuhai 519082, China (e-mail: zhangwm25@mail.sysu.edu.cn).

Guoqing Zhou is with the Guangxi Key Laboratory of Spatial Information and Geomatics, Guilin University of Technology, Guilin 532100, China (e-mail: glitezhou@yahoo.com).

Felix Morsdorf is with the Remote Sensing Laboratories, Department of Geography, University of Zurich, CH-8057 Zurich, Switzerland (e-mail: felix.morsdorf@geo.uzh.ch).

Digital Object Identifier 10.1109/JSTARS.2021.3130738

Index Terms—Clumping effect, full-waveform, leaf area index (LAI), LiDAR, occlusion effect.

I. INTRODUCTION

LEAF area index (LAI) is a crucial vegetation structural parameter in modeling terrestrial ecosystems [1]–[3]. Spaceborne full-waveform LiDAR provides data with great potential for LAI retrieval due to the direct measurement of the vertical canopy structure at a near-global scale, while being less prone to saturation problems in dense forest (compared with passive optical remote sensing) [4]–[6]. The demand for deriving LAI from spaceborne LiDAR is increasing with the increasingly available data from the Geoscience Laser Altimeter System (GLAS) [7], Global Ecosystem Dynamics Investigation (GEDI) [4], [8], and the upcoming Multi-footprint Observation LiDAR and Imager (MOLI) [9].

Empirical methods and physically-based models were used for LAI retrieval. Luo *et al.* [10] proposed an empirical method, which relies on field-measured LAI, to retrieve LAI from GLAS data. However, this approach is unsuitable for LAI retrievals over large areas and lacks a physical basis [11]. Beer's Law [12] was directly applied to footprint gap probability to retrieve LAI [13]; this is the current approach used for LAI products [14] from spaceborne LiDAR. Effective LAI (LAI_e) is retrieved in such a way by assuming that the distribution of canopy

components in the footprint is homogeneous. The non-linearity of Beer's law, in addition to the heterogeneous distribution of canopy components (i.e., clumping) in the footprint, leads to an underestimation of LAI [2], [11]. In ground-based LAI measurement, the underestimation might range from 30% to 70% in forests with highly clumped leaves [15]–[17]. As a footprint (65 m for GLAS) generally covers several tree crowns and large gaps between crowns, Yang *et al.* [11] developed a method of correcting the heterogeneity caused by the between-crown gaps (i.e., between-crown clumping). Vertically projected fractional crown coverage estimated from passive optical Landsat imagery was used to segment the heterogeneous footprint into presumably homogeneous crown-covered regions and between-crown gaps. After applying Beer's law in the crown-covered regions, the retrieved LAI was converted to the whole footprint level. Compared to more than 30% underestimation when directly using Beer's law, this method significantly improved LAI retrieval. However, an apparent underestimation (bias = -0.49) between GLAS-derived and field-measured LAI was found due to the hypothesis that leaves are randomly distributed in the crown-covered regions [11]. Therefore, additional correction of within-crown clumping is an unsolved and highlighted issue to improve the LAI retrieval from large-footprint LiDAR.

The measurement characteristics of spaceborne LiDAR make it difficult to apply methods, developed to correct the clumping effect in ground-based LAI measurement, to LAI retrieval from space-borne instruments. The classical clumping effect correction methods include the finite-length averaging method [18], gap-size distribution method [15], [19], combination of gap-size distribution and finite-length averaging method [20], and the path length distribution (PATH) method [21], [22]. The first three methods have been widely used in indirect ground LAI measurements; however, they are not suitable for correcting the clumping in large-footprint full-waveform LiDAR data due to the lack of detailed gap distribution information [21]. Spaceborne full-waveform LiDAR records (near-) vertical echo information at a fixed sampling interval (usually 0.15 m, corresponding to a measurement rate of 1 ns for most laser instruments), as the laser pulse interacts with the higher to lower canopy parts and finally with the ground. However, each return is a composition of the integrated reflections from a relatively large field of view (i.e., within the laser footprint) within the sampling interval [23]. It is impossible to resolve the gap distribution information within the footprint, turning the clumping correction into an ill-posed problem needing ancillary information to be solved. PATH method uses the relative path length distribution, the probability density function of a specific path length that the ray passes through the canopy [22], to characterize the heterogeneity in the crown-covered regions. In LAI retrieval from discrete airborne laser scanning (ALS) point clouds data, the fraction of vertically projected canopy coverage [24] was used to correct between-crown clumping. The relative path length distribution was derived from a Canopy Height Model (CHM) reflecting the three-dimensional (3D) foliage profile [21]. However, how to derive the relative path length distribution from large-footprint

full-waveform data has not been addressed so far. PATH can potentially be used to correct the within-crown clumping further in spaceborne LAI retrieval if we can obtain the canopy profile information from the waveform.

The vertical structure information measured by waveform LiDAR has not been fully utilized in clumping effect correction; usually, only the two-dimensional gap probability estimated from the waveform [25] is used in current footprint-level LAI retrievals [11]. Canopy characteristics in the path of the laser beam influence the shape of the backscattered signals. Correspondingly, the returned waveform should potentially yield information on the vertical canopy profile [26]. However, we cannot directly derive the vertical canopy profile from the waveform due to the occlusion [27]–[29]. Canopy objects, which are further away from the LiDAR and possibly occluded by other canopy layers, will be under-represented in the digitized waveform [30]. Occlusion correction would be a major step forward to realize a proper representation of vegetation structure and exploit the full potential of full-waveform data [31]. However, the limited existing studies are either for small-footprint discrete return [32] or for full-waveform ALS data [30], [33], [34], which have different constraints and relevant scales of occlusion compared to the large-footprint waveform. To our knowledge, occlusion correction methods for large-footprint waveform data are still not available operationally. An approach of compensating the occlusion of higher vegetation layers is needed to resolve the vertical canopy profile. In addition, how to derive relative path length distribution from the canopy profile is critical to correct the within-crown clumping.

In terms of validation, although field-measured data provide reference values, using real-world data in rigorously evaluating and diagnosing issues [35] in LAI retrievals is challenging. It is difficult to obtain a systematic variation in canopy architecture from field data, and the experimental errors can become convoluted with model errors. On the contrary, computer simulation is convenient in generating diverse canopies. Still, it has not been widely used in evaluating the performance of current LAI retrieval algorithms from large-footprint full-waveform LiDAR. With the development of radiative transfer models [36]–[39], the full-waveform data and the actual LAI of the virtual scenes can be synergistically acquired, supporting research using simulated data.

This study explored the possibilities in improving LAI retrieval accuracy from large-footprint full-waveform LiDAR data by further correcting the within-crown clumping. We

- 1) proposed a method of correcting occlusion in canopy waveform to obtain the vertical canopy profile;
- 2) developed a method of deriving relative path length distribution from the occlusion corrected waveform and corrected the within-crown clumping in LAI retrieval; and
- 3) evaluated the performance of our and the other two current physically-based methodologies (i.e., applying Beer's law directly and correcting the between-crown clumping) based on simulated (with known true LAIs) and GLAS waveform data (with field-measured LAIs).

TABLE I
PROPERTIES OF THE DISCONTINUOUS CANOPIES

Discontinuous forests in a 25 m-diameter circular footprint		Abstract forests			Realistic forests	
Crown geometrical property	Shape	Cylinder	Sphere	Cone	<i>Citrus</i>	<i>Oak</i>
	Diameter (m)	4	4	4	5.62×5.18	6.03×5.85
	Crown length (m)	4	4	4-①, 8-②, 14-③	5.58	9.51
	Number	10	10	10, 16, 22	9, 6, 9	9, 6, 6
	Position	Randomly located	Randomly located	Randomly located	Random, clumped, regular	
Scatterer property	Leaf normal distribution	Uniform			Near uniform	
	Leaf scatter reflectance				0.50	
	Leaf scatter transmittance				0.44	
	Background reflectance				0.25	
	Scattering law of leaf and background				Bi-Lambertian	
Crown structural property	Leaf Area Density (ρ) (m^2/m^3)	0.25 0.50 0.75 1.00 1.25 1.50	0.25 0.50 0.75 1.00 1.25 1.50	0.25 0.50 0.75 1.00 1.25 1.50	1.61	1.08
	Leaf Area Index (LAI) (m^2/m^2)	1.00 2.00 3.00 4.00 5.00 6.00	0.67 1.33 2.00 2.67 3.33 4.00	① 0.33 0.67 1.00 1.33 1.67 2.00	3.12	6.18
				② 0.67 1.33 2.00 2.67 3.33 4.00		
				③ 1.17 2.33 3.50 4.67 5.83 7.00		
	Clumping Index (Ω) (0°)	0.96 0.99 0.99 1.01 1.02 1.04	0.95 0.94 0.91 0.90 0.87 0.85	① 0.94 0.89 0.88 0.84 0.80 0.78	0.74	0.59
				② 0.91 0.83 0.77 0.72 0.67 0.63		
③ 0.86 0.74 0.67 0.59 0.54 0.50						

II. MATERIALS

A. Simulated Full-Waveform Dataset

To precisely model interactions with LiDAR pulses, the parameterization of the LiDAR waveform model needs two kinds of input: the parameters of the virtual laser instrument and the canopy structural attributes.

The laser instrument parameters were: 1) Gaussian power distribution in space with the intensity decreasing to $1/e^2$ of its peak value at the 25-m footprint diameter; 2) 5 ns pulsewidth, roughly resemble GLAS (4 ns) [40] and MOLI (<7 ns) [9]; 3) Measuring the objects at 0° zenith angle using a wavelength of 1064 nm, with a measurement rate of 1 ns.

The canopy structural attributes were generated from Discrete Anisotropic Radiative Transfer (DART) model [38], [41] and OnyxTREE¹, which include: (i) abstract discontinuous cylindrical, spherical, and conical canopies with between-crown gaps in a 25-m diameter footprint, constructed from randomly distributed leaf facets (details in Table I: abstract forests); (ii) realistic discontinuous canopies with *Citrus* trees from RAMI IV², *Oak* trees from OnyxTREE, and a hybrid scene (details in Table I: realistic forests). The distance between the bottom of the canopy and the ground was set to be 5 m. The geometrical scenes are shown in the result section.

1) *Abstract Discontinuous Canopies*: Leaves with a square shape and an area of $0.05 \times 0.05 \text{ m}^2$ (used in [42]) were randomly distributed within cylindrical, spherical, and conical tree crowns. We generated six different values of Leaf Area Density (ρ , unit: m^2/m^3), the one-sided leaf area per volumetric unit [43], ranging from 0.25 to 1.50 (the ρ used in previous studies ranges from 0.25 to 1.59 [35], [42], [44], [45]) with an increment of 0.25. Both sides of the leaf surface and the ground

were all set to bi-Lambertian. The reflectance and transmittance of foliage and the ground surface reflectance were set to be 0.50, 0.44, and 0.25, respectively (same as the experiment in RAMI IV: HET22_DIS_UNI_NIR_20). The orientations of the leaf elements (scatterers) followed a spherical distribution ($G = 0.5$). We generated 10, 16, and 22 cones randomly located in the footprints to construct abstract discontinuous canopies, which were used to test the performance of the method when the ρ and the fractional crown coverage (f_{cover}) vary in the footprint. Table I provides the detailed properties of the crowns and the scatterers for the vegetation parameterization in DART.

2) *Realistic Discontinuous Canopies*: We generated nine realistic discrete canopy scenes with random, clumped, and regular distributions of trees (*Citrus* and *Oak*) in the 25-m diameter footprints. The spatial distributions of leaves in the crowns were non-uniform. The crown diameters were $5.62 \text{ m} \times 5.18 \text{ m}$ (east-west) for the *Citrus* and $6.03 \text{ m} \times 5.85 \text{ m}$ (east-west) for the *Oak*. The crown lengths (i.e., distance from top to bottom of the crown) were 5.58 and 9.51 m for the *Citrus* and *Oak*, respectively. Branches were not included in the waveform simulation. Table I provides detailed information on the trees, scenes, and spectral parameters (the reflectance, transmittance of the leaf, and the reflectance of the underlying ground).

In total, we generated 65 scenes, including five different crown lengths (4, 8, and 14 m for abstract trees; 5.6, 9.5 m for realistic trees), four experiments with varying numbers of trees in the footprint (9, 10, 16, 22), and eight kinds of ρ (varying from 0.25 to 1.50 with an increment of 0.25 for abstract trees, and 1.6, 1.1 for the realistic trees).

B. Real Full-Waveform Data

We used 17 GLAS footprints of forests on flat terrain (using data from [11] with the slope angle less than 5 degrees) located in Linzhi County, on the Tibetan Plateau of China ($93^\circ 50' - 94^\circ 40'$, $29^\circ 00' - 29^\circ 50'$) to test the performance of the methods. The

¹[Online]. Available: <http://www.onyxtree.com/>

²[Online]. Available: <https://rami-benchmark.jrc.ec.europa.eu/HTML/RAMI-IV/RAMI-IV.php>

TABLE II
METHOD OF MODIFYING THE RETURN SIGNALS IN THE CANOPY

R_i : the laser energy returns from a certain layer	R_i^* : Theoretical corresponding R_i when without upper vegetation	Actual modification from R_i to R_i^*
$R_1 = (Q_0 f_{cover}) \frac{1-t_1}{f_{cover}} \rho_v$ ① ② ③	$R_1^* = Q_0 (1-t_1) \rho_v$ ④ ⑤ ③	$R_1^* = R_1$
$R_2 = [(Q_0 f_{cover}) \frac{P(z_1) - (1-f_{cover})}{f_{cover}}] \frac{1-t_2}{f_{cover}} \rho_v$ ① ② ③	$R_2^* = Q_0 (1-t_2) \rho_v$	$R_2^* = \frac{R_2}{\frac{P(z_1) - (1-f_{cover})}{f_{cover}}}$
...
$R_n = [(Q_0 f_{cover}) \frac{P(z_{n-1}) - (1-f_{cover})}{f_{cover}}] \frac{1-t_n}{f_{cover}} \rho_v$ ① ② ③	$R_n^* = Q_0 (1-t_n) \rho_v$	$R_n^* = \frac{R_n}{\frac{P(z_{n-1}) - (1-f_{cover})}{f_{cover}}}$

① Incident energy on the crown-covered regions in a certain layer; ② Interception rate of the vegetation in crown-covered regions in a certain layer; ③ Reflectivity of the canopy components in a certain layer.
④ Incident energy on a certain layer; ⑤ Interception rate of a certain layer.

forest was an open canopy with nearly mature trees, which grow slowly and mainly comprise *Pinus densata*, *Picea spinulosa*, and *Betula platyphylla* Suk. The data includes 1) GLAS original waveform data acquired by the Laser 3J campaign in March 2008; 2) Landsat-5 Thematic Mapper imagery used as auxiliary data for the fractional crown coverage (f_{cover}) estimation; 3) corresponding LAI of the GLAS footprints measured by Tracing Radiation and Architecture of Canopies (TRAC; 3rd Wave Engineering, ON, Canada) in July 2011, with 200–300 m back and forth line samplings in each plot. In addition, TRAC-measured LAIs were calculated based on the gap size distribution method [15], [19]; the woody components, the leaf angle distribution [46], [47], and the needle-to-shoot level clumping were not considered. The ratio of canopy reflectance to that of the ground was set to be 2.0 [11] in the estimation of the gap probability of the footprint. Other detailed information about the data acquisition, method of data processing, and illustration of the study area were included in [11].

III. METHODS

In current physically-based models of LAI retrieval (LAI_e and $LAI_{e-f_{cover}}$, details in Table III, Appendix A) from spaceborne full-waveform LiDAR, path lengths of the laser beams passing through the materials in the entire footprint and through the crown-covered regions are assumed to be equal [Table III (a), (b)], which is not the case in the real forest [Table III (c)]. PATH method [2], [21], [22] considers variable path lengths in the ground- and ALS-based LAI measurement; LAI_{PATH} (Appendix B) can be retrieved by using the relative path length distribution ($p(l_r)$) to correct the within-crown clumping further. In this section, we proposed a method of deriving $p(l_r)$ from the waveform to realize the correction of within-crown clumping,

after the occlusion in the waveform was compensated using our proposed occlusion correction method. After correcting both the between-crown and within-crown clumping, the retrieved LAI_{PATH} was compared with LAI_e and $LAI_{e-f_{cover}}$.

Our methods include 1) a method of correcting the occlusion in the canopy return signal, using the original waveform [Fig. 1(1)], gap probability profile of the footprint [Fig. 1(2)], and fractional crown coverage (Fig. 1(3)); 2) a method of deriving $p(l_r)$ from the occlusion corrected waveform [Fig. 1(4)–(6)]; 3) validation and comparison of the three kinds of physically-based models for LAI retrieval [Fig. 1(8)], from not correcting any clumping to correcting both the between-crown and within-crown clumping. In addition, the modified waveform and $p(l_r)$ were validated using actual vertical leaf area (viewed as the true vertical canopy profile) and ray tracing, respectively.

A. Mechanism of Radiation Transfer in LiDAR

In the LiDAR equation [48]–[50]

$$R = \frac{Q_t D_r^2 \Gamma}{4\pi s^4 \beta_t^2} T^2 \sigma \quad (1)$$

$$\sigma = \frac{4\pi}{\Omega} \rho A_s \xrightarrow{\text{Lambertian assumption}} \sigma = 4\rho_d A_s \quad (2)$$

where R is the power entering the receiver, Q_t is the transmitted power, D_r is the aperture diameter of the receiver optics, β_t is the beam divergence, s is the distance between the laser scanner and the scatterer, Γ is the optical efficiency of the system, T is the atmospheric transmission loss; σ is the backscatter cross-section, Ω is the solid angle, ρ is the biconical reflectance, ρ_d is the diffuse reflectance (often referred to as reflectivity), and A_s is the projected receiving area of the scatterers. In LiDAR remote sensing, the scattering surface is usually assumed to act

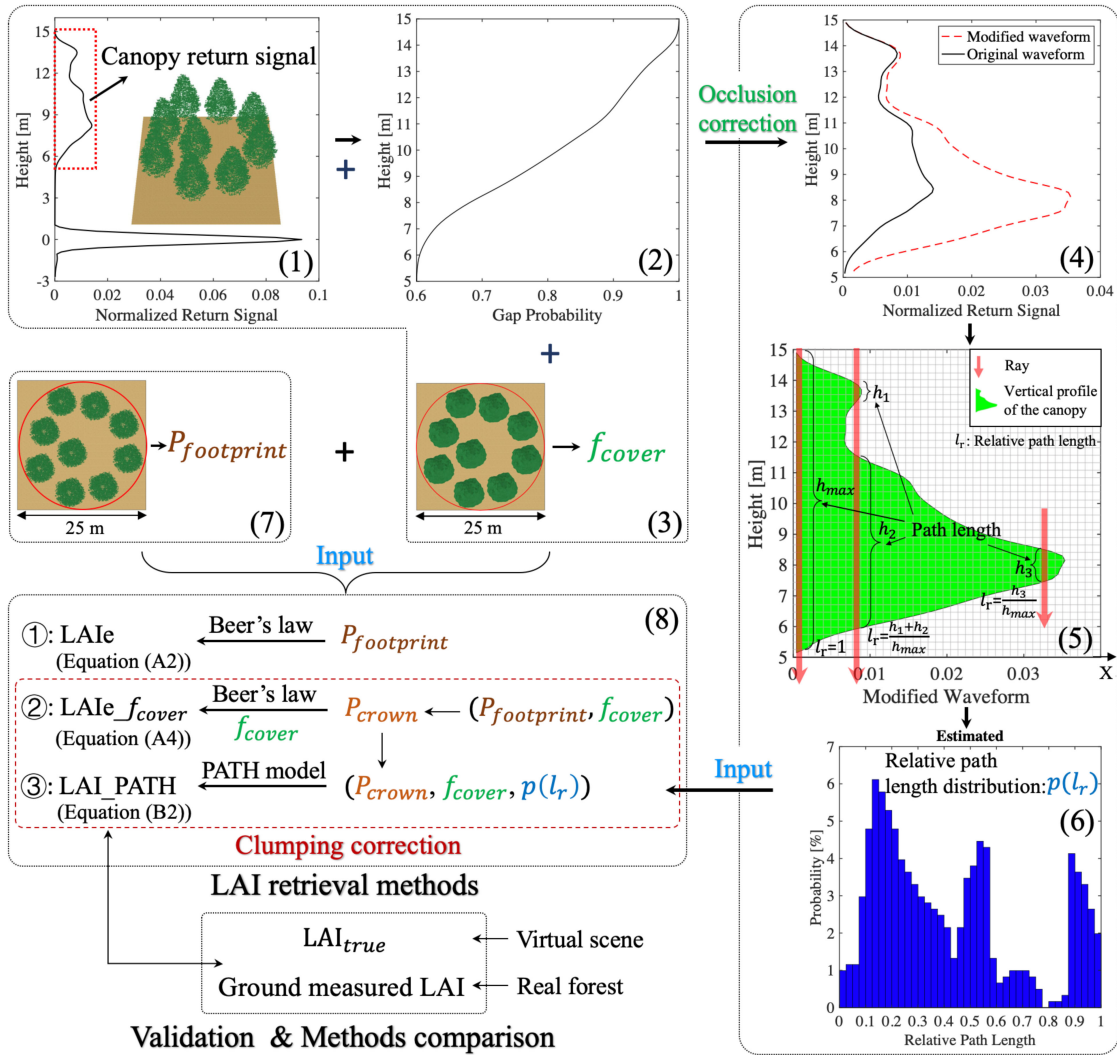


Fig. 1. Workflow diagram for LAI retrieval from the waveform: (1) the original waveform, normalized by the sum of all returns; (2) gap probability from the top to the bottom of the canopy (Section III-C); (3) the fractional crown coverage (f_{cover}) in the footprint; (4) the modified waveform by using (1), (2), and (3) (Section III-B); (5) the method of obtaining the relative path length distribution ($p(l_r)$) of the canopy from the modified waveform (Section III-D), and (6) the estimated $p(l_r)$ from (5); (7) the gap probability of the footprint ($P_{footprint}$); (8) LAI retrieval from not correcting any clumping (LAI_e , details in (A2), Appendix A), correcting the between-crown clumping ($LAI_e f_{cover}$, details in (A4), Appendix A), and correcting both between-crown and within-crown clumping (LAI_{PATH} , details in (B2), Appendix B), respectively.

Lambertian, so ① is simplified to ②. It is noted from (1) and (2) that the reflected power R depends on two types of variables. One set of variables is linked with the measurement process, including the laser scanner, receiver optics, and the atmosphere parameters. The other set is linked with the scatterer, i.e., the reflectivity (ρ_d) and the receiving area (A_s). If we neglect the influence of the atmosphere and the variation in vegetation reflectance, A_s is the main contributing factor affecting the magnitude of R . In addition, R in (1) is “instantaneous,” while in reality, it is time (distance) dependent (see schematic diagram of R in Fig. 2).

Spaceborne LiDAR is sensitive to the vertical distribution of intercepted scatterers, and the recorded waveform amplitude reflects the strength of the return. Larger amplitude indicates more canopy components for surfaces with similar reflective properties and geometry within a footprint [51]. Therefore, measured R of a specific vegetation layer should correspond

to the amount of canopy components, i.e., foliage elements. However, we cannot use this information directly because the incident energy in the lower canopy is affected by the upper canopy, namely through the occlusion. Thus, we proposed a method of correcting the occlusion.

B. Method of Correcting Occlusion for the Canopy Waveform

When the laser beam can penetrate the forest, the idea of correcting the return signal is to invert the attenuation process using a correction factor, asserting what a lower canopy return could be without the occluding upper layers. For most current LiDAR systems, the measurement setup is monostatic (i.e., transmitter and receiver share the same optical path), which makes LiDAR measuring in the so-called “hot spot” [52]. Therefore, a one-way attenuation model is used since a scattering surface that the transmitted laser energy can reach will also be

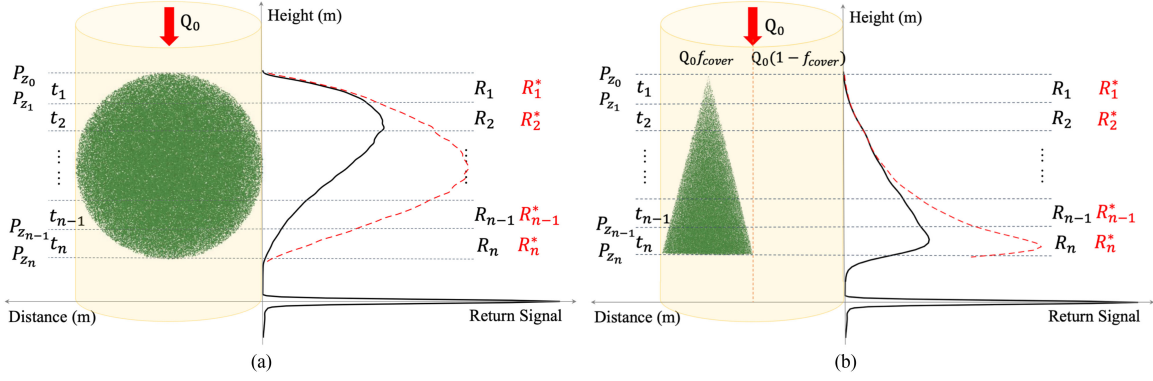


Fig. 2. Schematic diagram of the LiDAR measurement and the modification of the return signals: (a) continuous canopy; (b) discontinuous canopy. The solid black line denotes the original return signals, and the red dotted line represents the modified signals for the canopy. The explanation of the symbols and the method of modifying the return signals are in Table II.

visible to the receiver [25]. The basic assumption is similar to that proposed by Ni-Meister *et al.* [25]: the gap probability is the complement of the vertical canopy profile as laser energy can only penetrate the lower layer through gaps (including both within-crown and between-crown gaps), while multiple scattering is not considered. Thus, with a known gap probability above a certain height $P(z_{i-1})$ and the measured return signal R_i affected by the occlusion effect, the potential returned energy R_i^* can be obtained from the equations listed in Table II:

i is the id of the vegetation layer, which varies between 1 to n , where 1 and n refer to the top and the bottom vertical layer of the canopy, respectively. R_i is the LiDAR measurement within a specific sampling interval, which is usually set to be 1 ns, corresponding to a height of 0.15 m, indicating that we can obtain a measurement every 0.15 m; Q_0 is the atmospherically corrected laser pulse energy, f_{cover} is the fractional crown coverage, t_i means the total gap probability of the i th vertical layer but is unnecessary in the final equation from the measured R_i to the modified laser energy returns R_i^* . $P(z_i)$ means the gap probability above a certain height z_i . The corresponding method of estimating $P(z_i)$ is illustrated in Section III-C.

It is noted from Fig. 2 that if there are between-crown gaps in the footprint, the total incident energy can be divided into two parts: one can directly reach the ground, $Q_0(1-f_{cover})$; and the other is the energy incident on the crown-covered regions, $Q_0 f_{cover}$. Note that the fraction of the incident energy influenced by the transmission loss varies with the canopy height because of the conical or spherical shape of the canopy, but only the total projected f_{cover} can be obtained by passive optical remote sensing data. Thus, $Q_0 f_{cover}$ is used to approximately denote the total part of incident energy in the footprint that is subject to transmission losses in the path of the laser beam. In addition, $\frac{1-t_i}{f_{cover}}$ is the interception rate of the vegetation in crown-covered regions in the i th layer, and, $\frac{P(z_{i-1})-(1-f_{cover})}{f_{cover}}$ is the within-crown gap probability above the height z_{i-1} , defined as the proportion of the laser beam passing through the crowns above the height z_{i-1} without being scattered, $(Q_0 f_{cover}) \frac{P(z_{i-1})-(1-f_{cover})}{f_{cover}}$ is the incident energy on crown-covered regions in the i th layer. For the energy entering the receiver (the two-way transmission losses in the atmosphere and the response function of the receiver

are not considered), the reflected energy approximately equals the incident energy multiplied by the interception rate and the reflectivity of the canopy components in this layer. In the second column of Table II, R_i^* refers to the potentially reflected energy as if the lower vegetation layer is not affected by the upper canopy, so the equation of the R_i^* is very concise because the incident energy is always Q_0 . Comparing the first and the second column, the returned energy unaffected by the occlusion effect can be obtained with the equations in the third column using the gap probability profile information, f_{cover} , and the actual R_i . Then, the modified energy R_i^* is directly proportional to the receiving area $A_{s_i}^*$:

$$\begin{aligned} R_i^* &\propto A_{s_i}^*; A_{s_i}^* \propto \text{the amount of foliage elements} \\ &\Rightarrow R_i^* \propto \text{the amount of foliage elements} \end{aligned} \quad (3)$$

where $A_{s_i}^*$ is the receiving area of the i th layer unaffected by the occlusion of the upper layers, corresponding to A_{s_i} . It is reasonable to assume that if there is a larger $A_{s_i}^*$ in specific vertical vegetation layer, there are more foliage elements in this layer. Therefore, the modified waveform (i.e., many values of R_i^*) reflects the vertical canopy profile.

C. Method of Estimating the Gap Probability (Profile)

We estimated the vertically resolved directional gap probability of an individual footprint using the vertical canopy energy distribution and ground energy [4], [25]. To distinguish vegetation and ground signals, the waveform was decomposed into a series of Gaussian peaks using a Gaussian decomposition method [53]. In addition, the detection of inflection points and the Levenburg-Marquardt Least Squares technique [54] were used to initialize and adjust the parameters in Gaussian fitting. The last peak was assigned to be the ground surface, and other components were considered the canopy returns.

Equation (4) proposed by Ni-Meister *et al.* [25] is widely used to estimate the gap probability at a specific height z

$$P(z) = 1 - \frac{R_v(z)}{R_v(0)} \frac{1}{1 + \frac{\rho_v}{\rho_g} \frac{R_g}{R_v(0)}} \quad (4)$$

where $R_v(z)$, $R_v(0)$, and R_g are the laser energy returns from the canopy top to height z , from canopy top to ground, and from the ground return individually [25]. The ratio of the reflectance of the forest canopy (i.e., overstory canopy) and background (i.e., shrub, grass, or bare earth), $\frac{\rho_v}{\rho_g}$, changes with the leaf orientation factor and spectral properties of the foliage elements and the background; it is difficult to be obtained from single-wavelength LiDAR alone and is usually assumed to be a fixed value [10], [11], [13]. This inevitably causes uncertainty in $P(z)$ retrieval, depending on reflectance heterogeneity of forest canopy and background, which show the anisotropic variations due to the observation geometry. Besides, although the foliage reflectance is known, it is hard to obtain the canopy reflectance for the virtual scenes. It indicates that the true $P(z)$ cannot be derived from the simulated waveform.

Inspired by equations in [55], the relationship between R_g and $P(0)$ (gap probability of the footprint) is

$$R_g = Q_0 P(0) \rho_g; P(0) = 1 - \frac{R_v(0)}{Q_0 \rho_v}. \quad (5)$$

Equation (4) becomes

$$P(z) = 1 - \frac{R_v(z)}{R_v(0)} \frac{1}{1 + \frac{R_g}{Q_0 \rho_g - R_g}} \quad (6)$$

where $Q_0 \rho_g$ is the reflected energy from the pure ground where there is no vegetation, and the $\frac{\rho_v}{\rho_g}$ is no longer needed in $P(z)$ calculation.

For the simulated data, the waveform of a pure ground, where ρ_g is the same with that when there are trees in the footprint, was simulated to acquire the $Q_0 \rho_g$. $Q_0 \rho_g$ was used to retrieve the $P(z)$ of a vegetation footprint based on (6); thus, $P(z)$ is close to the true gap probability profile. This is to avoid the impact of the uncertainty of $P(z)$ on evaluating the theoretical performance of the LAI retrieval method using synthetic data. For the GLAS data, it is difficult to find the pure ground footprint in the forests. In addition, we aimed to have a comparison between $\text{LAI}_{e_f_cover}$ in a previous study ([11], where $\frac{\rho_v}{\rho_g}$ is assumed to be 2.0) and our derived LAI_{PATH} . Therefore, $P(z)$ is estimated based on (4) using the same $\frac{\rho_v}{\rho_g}$ (i.e., 2.0) as [11].

D. Estimating Relative Path Length Distribution

The original return signals are composed of two parts: the canopy and the ground. We obtained the canopy waveform by splitting the original waveform based on the canopy base height. For the simulated waveforms, the canopy base height was 5 m, the distance between the bottom of the canopy and the ground for the virtual scenes. We found from the simulated waveforms that the canopy base height was located around the bottom of the second last Gaussian component, which was at the location of $\mu_{n-1} - 2\sigma_{n-1}$. In the Gaussian fitting, $y = \sum_{i=1}^n A_i e^{-\frac{(x-\mu_i)^2}{2\sigma_i^2}} + \varepsilon$, where y is the fitted waveform, x is the elevation, ε is the noise level of the waveform, n is the number of the Gaussians, A_i , μ_i , and σ_i are the amplitude, elevation position (i.e., the center), and half-width (standard deviation) of the i th Gaussian component [11], respectively. The elevation

of the ground peak (the n th Gaussian component) was set to 0. For the real-world waveform data, the canopy base height was automatically identified as the location of $\mu_{n-1} - 2\sigma_{n-1}$. The modified waveform [Fig. 1(4)] was assumed to be the vertical profile of the canopy and was closed (i.e., to the value of the first return signal, which is usually close to zero). Then, Fig. 1(5) was rasterized to calculate the relative path length distribution: 1) establishing a statistic of the height (h , i.e., the path length) of the rays passing through the canopy profile column-by-column in the modified signal direction (i.e., x -axis direction); 2) converting the height value in each column to relative path length (l_r), $l_r = h/h_{\text{max}}$, so that each column stores a l_r ; 3) computing the relative path length distribution of the canopy based on the following equation [21]:

$$p(l_r) = \frac{\hat{p}(l_r)}{\int_0^1 \hat{p}(l_r) d(l_r)} \quad (7)$$

where $\hat{p}(l_r)$ is the frequency of l_r falling within the interval $[l_r, l_r + d(l_r)]$, $d(l_r) = 0.025$, and is the number of columns in Fig. 1(6), which satisfy this condition, $\int_0^1 \hat{p}(l_r) d(l_r)$ is the total number of columns of which $l_r > 0$.

With known relative path length distribution, the gap probability, and fractional crown coverage, we can retrieve the “true” LAI using PATH. As a result, most of the clumping effects are removed.

E. Validation and Methods Comparison

Validating the modified waveform is challenging because it is hard to know the return signals without attenuation. Thus, we performed the validation by assuming the distribution of the leaf area of the virtual scene in the vertical direction approximately represents the profile of the canopy. We calculated the vertical leaf areas in 0.15-m height intervals via DART and normalized them by the sum of the total leaf area between the top and bottom of the canopy. Then, we compared the vertical leaf area profile with the modified waveform, which was normalized by the sum of all the modified signals.

To validate the relative path length distribution, we used the ray-tracing method to acquire the true values. We calculated the lengths of rays intersecting the envelopes of the abstract crowns by sending vertical rays (100 rays/m²) to the scene using LESS (Large-Scale remote sensing data and image simulation framework) [36]. The path length is zero when the ray hits the ground directly through the between-crown gaps. We only considered the rays with path lengths over zero in the statistic.

We tested the difference of the retrieved LAI using three kinds of physically-based methods. They include LAI_e (not correcting the clumping in the footprint, see (A2) in Table III), $\text{LAI}_{e_f_cover}$ (correcting the between-crown clumping only, see (A4) in Table III), and LAI_{PATH} (correcting both the between-crown and within-crown clumping, see (B2) in Appendix B). The relative errors of LAI were calculated as follows:

$$\Delta_j = \frac{\text{LAI}_j - \text{LAI}_{\text{true}}}{\text{LAI}_{\text{true}}} \cdot 100\%; j = 1, 2, 3 \quad (8)$$

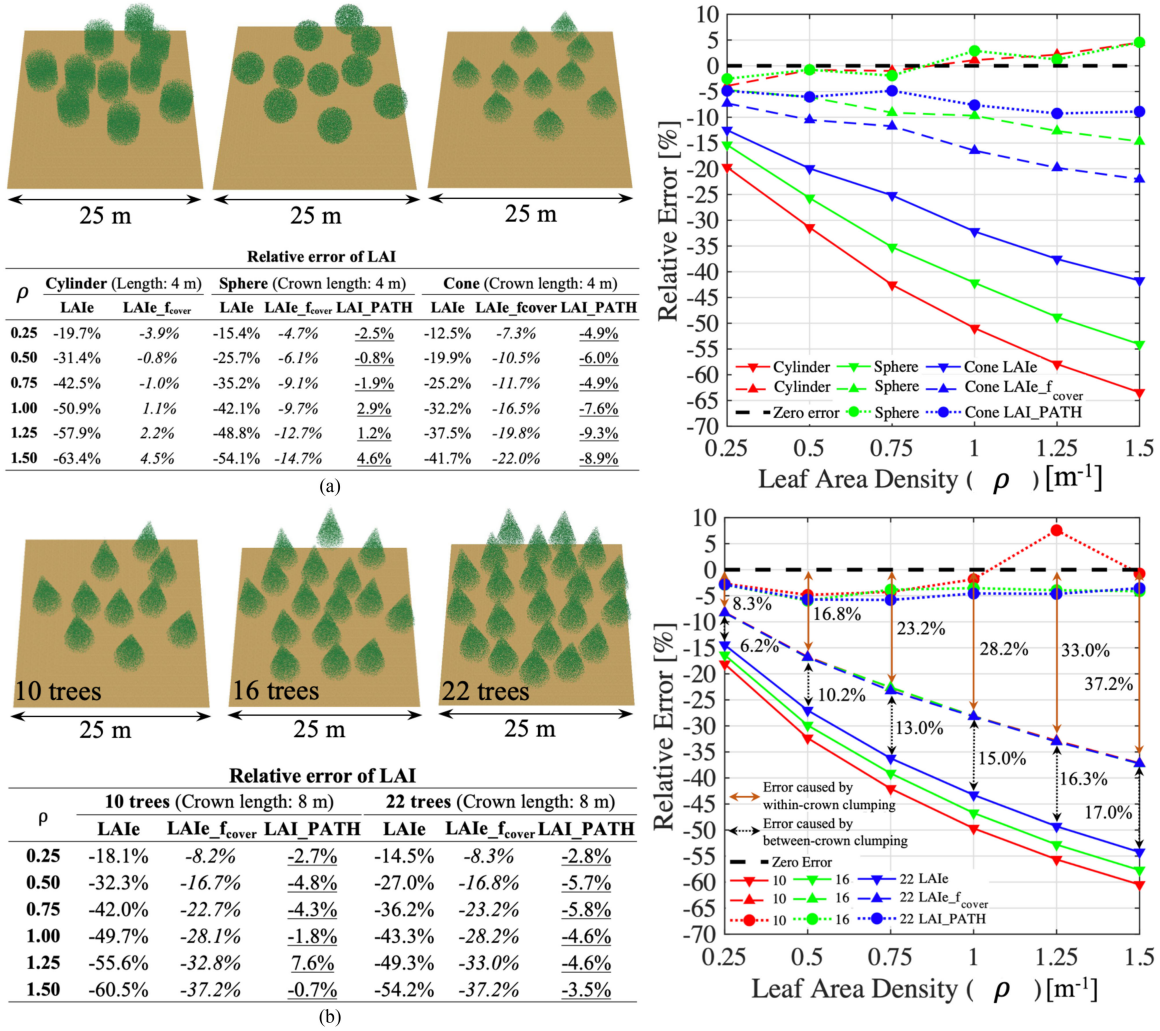


Fig. 3. Geometrical scenes when the leaf area density (ρ , unit: m^2/m^3) is 0.75 and the relative errors of LAI from directly applying Beer's law (LAI_e), correcting the between-crown clumping (LAI_{e_fcover}), and correcting both the between-crown and the within-crown clumping (LAI_{PATH}) for discontinuous canopies with the crown ρ ranging from 0.25 to 1.50: (a) comparison of scenes with same ρ and same crown length, but different crown shape (red denotes the cylinder, green denotes the sphere, and blue denotes the cone); (b) comparison of conical scenes with same ρ and same crown length, but different fractional crown coverage (f_{cover}).

where $j = 1, 2, 3$, Δ_j corresponds to the relative error of LAI_e (Δ_{LAI_e}), LAI_{e_fcover} ($\Delta_{\text{LAI}_{e_fcover}}$), and LAI_{PATH} ($\Delta_{\text{LAI}_{PATH}}$), respectively. LAI_{true} can be calculated accurately in the virtual scenes.

We used the three methods to retrieve LAI from simulated waveform data of virtual scenes and GLAS data. For synthetic scenes, the reference true values of required parameters for LAI retrieval, including the gap probability at crown-covered region (P_{crown}) and fractional crown coverage (f_{cover}) were used to test the theoretical performance of the methods. Specifically, gap probability in the footprint ($P_{footprint}$) and f_{cover} were calculated from the total vertical projected shadow of leaves, and the crown envelopes, in the footprint, respectively. For the GLAS data, same with methods in [11], $P_{footprint}$ was calculated from the waveform, and f_{cover} was estimated from Landsat imagery.

Moreover, the performance of the three methods in various crown shapes, leaf area densities, crown lengths, and fractional crown coverages was tested using abstract virtual canopies.

IV. RESULTS

A. LAI Retrieval of Abstract Discontinuous Canopies

Different scenes were generated to test the performance of the three methods with different crown shapes [Fig. 3(a)], various leaf area densities, crown lengths [conical canopies in Fig. 3(a) and (b)], and f_{cover} (i.e., different number of trees) [Fig. 3(b)]. The results show that the overall performance is: $\text{LAI}_{PATH} > \text{LAI}_{e_fcover} > \text{LAI}_e$. The accuracy is greatly improved after correcting both the between-crown and within-crown clumping; errors of LAI_{PATH} are below 10% for all scenes (Fig. 3). Specifically, the performance of the three methods is summarized as follows.

- 1) LAI_{PATH} is not affected by the crown ρ . On the contrary, the errors of LAI_e and LAI_{e_fcover} increase significantly with the crown ρ .

The underestimation of LAI_e and LAI_{e_fcover} is due to the nonlinearity of Beer's law, and the spatial

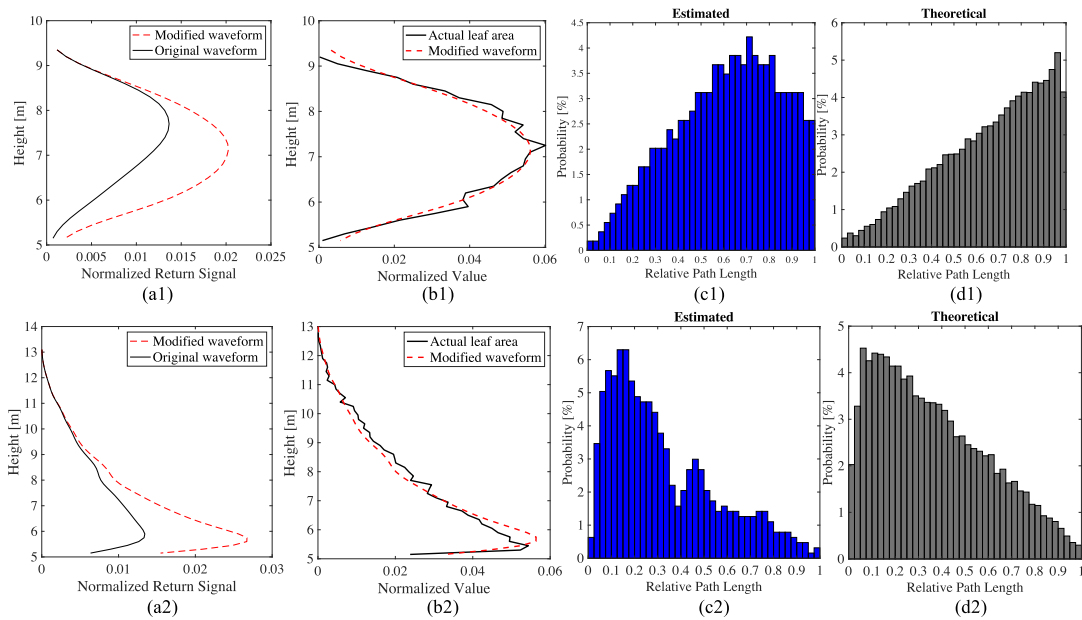


Fig. 4. Results of the discontinuous spherical and conical canopies with a crown length of 4 and 8 m (leaf area density (ρ , unit: m^2/m^3) is 0.75): (a) the original and the modified waveform for the canopy, (b) the comparison of the modified waveform and the normalized true vertical leaf area from DART, and (c) and (d) are the calculated relative path length distribution from the modified waveform and the ray tracing of the three-dimensional scenes, respectively.

heterogeneity in the footprint (for LAI_e) [11], [56] and crown-covered regions (for $\text{LAI}_{e_f_{\text{cover}}}$), which leads to the scale effect in LAI calculation [57]; LAI_PATH is not affected by the ρ because it considers the heterogeneity reasonably by using relative path length distribution. The heterogeneity caused by large gaps between crowns in the footprint increases with ρ and leads to a considerable underestimation in LAI_e ; the smaller the within-crown gap probability is, the greater the heterogeneity in the footprint level [11]. It explains why the error of LAI_e is the largest for cylindrical canopies (19.7–63.4%). On the contrary, the corresponding error of $\text{LAI}_{e_f_{\text{cover}}}$ is the most minor (less than 4.5%) because the cylinder is nearly homogeneous from the nadir view after removing the between-crown gaps. $\text{LAI}_{e_f_{\text{cover}}}$ significantly improves the LAI retrieval accuracy for the discrete cylindrical canopy; however, it is not that effective for canopy with other crown shapes. The error caused by within-crown clumping, which increases with the crown ρ , is non-negligible for the other kinds of canopy (Fig. 3). Different from LAI_e and $\text{LAI}_{e_f_{\text{cover}}}$, Beer's law is not applied directly on the entire footprint (as LAI_e) or heterogeneous crown-covered regions (as $\text{LAI}_{e_f_{\text{cover}}}$) in LAI_PATH , but on areas with similar gap probability (via similar path length) separately. As a result, LAI_PATH is not as much affected by the crown ρ , since it effectively mitigates the scale effect caused by directly applying the nonlinear Beer's law on heterogeneous regions. We also found that approximating the modified waveform as the vertical canopy profile yields good results in LAI retrieval.

- 2) LAI_PATH is less affected (error < 10%) by the crown length. The error of the other two methods is larger for

conical canopies with 8 m height (18.1–60.5% for LAI_e , 8.2–37.2% for $\text{LAI}_{e_f_{\text{cover}}}$) than 4 m height (12.5–41.7% for LAI_e , 7.3–22.0% for $\text{LAI}_{e_f_{\text{cover}}}$). It is because the longer the crown, the more considerable heterogeneity at nadir viewing of the crown area.

- 3) Different from LAI_e , LAI_PATH and $\text{LAI}_{e_f_{\text{cover}}}$ are not affected by f_{cover} (related to the number of trees in the scenes) because the between-crown clumping is corrected. The error of LAI_e decreases with the number of trees (from 10 to 22), as is noted in Fig. 3(b). The larger the f_{cover} , the more similar with a homogeneous canopy in the footprint.
- 4) Within-crown clumping correction is the most important for conical canopy. As is shown in Fig. 3(b), the error caused by within-crown clumping (8.3–37.2%) is significantly larger than the between-crown clumping (6.2–17.0%).

Fig. 4 shows the intermediate results in LAI_PATH calculation, which include the corresponding modified waveforms and relative path length distributions for the spherical canopy with ten trees [in Fig. 3(a)] and conical canopy with 16 trees [in Fig. 3(b)], when the crown ρ is 0.75.

Moreover, we tested the performance of the methods in more complex scenes with varying crown lengths and ρ values. The results show that the performance of LAI_PATH is less affected by the heterogeneity in crown length (error < 10%) (Fig. 5(a)), but the error increases if distinct ρ values are assigned to different crowns. However, the maximum LAI retrieval error is still less than 19% in such a case with considerable ρ heterogeneity (up to a three-times difference) in the footprint [Fig. 5(b)]. The errors of LAI_e (20.6–68.8%) and $\text{LAI}_{e_f_{\text{cover}}}$ (13.0–46.7%) are much larger than LAI_PATH in these complex scenes.

The intermediate results in the LAI_PATH calculation for the conical canopy with 22 trees [in Fig. 5(a)] and Scene 2 [in

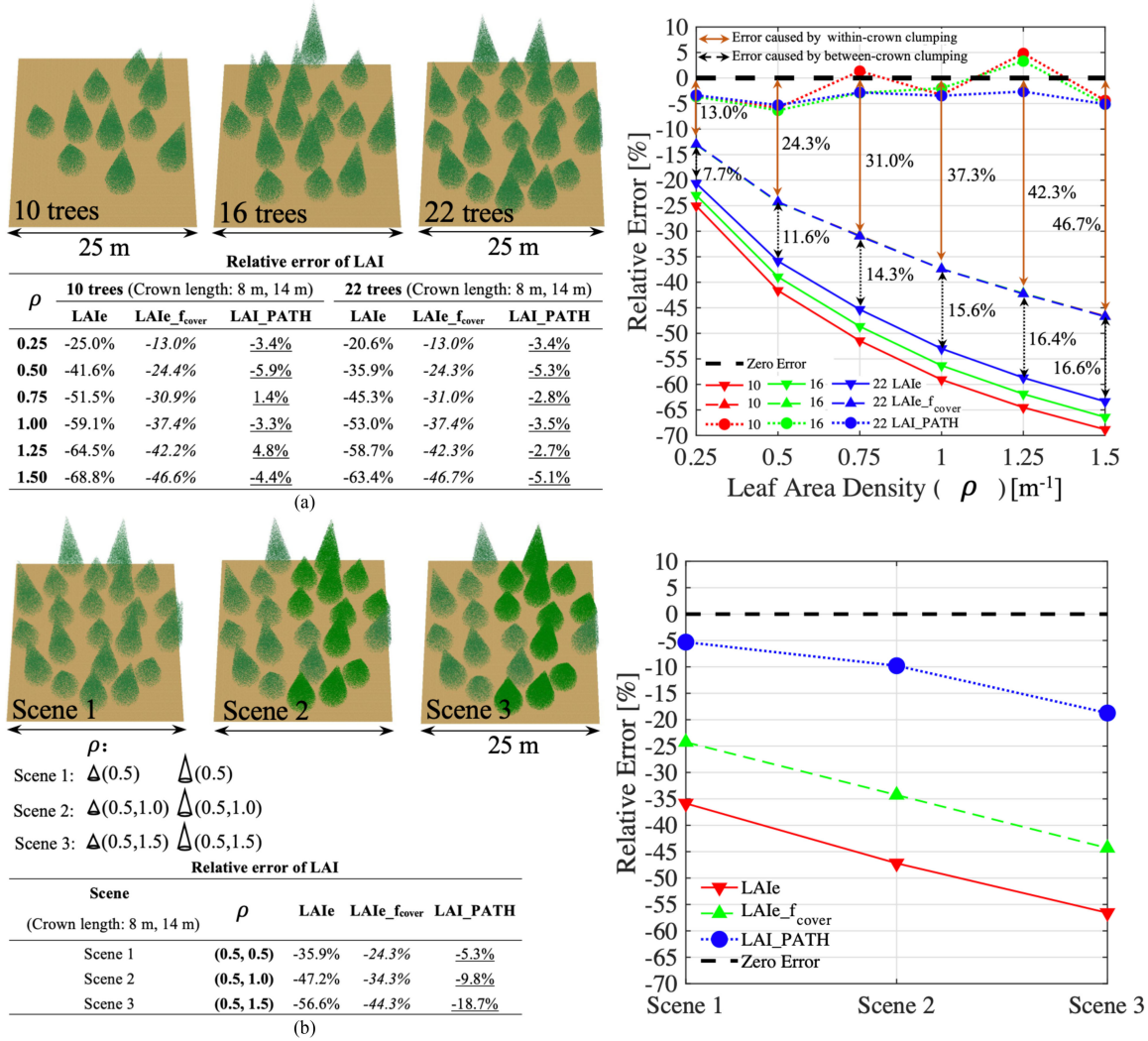


Fig. 5. Geometrical scenes and the relative errors of LAIs of the discontinuous conical canopies: (a) scenes with the same crown leaf area density (ρ , unit: m^2/m^3) but different length (8 m and 14 m), the geometrical scenes illustrate the cases when the ρ is 0.75; red, green, and blue denotes 10, 16, 22 trees in the footprint, respectively; (b) scenes with further heterogeneity in between-crown ρ than (a): crown ρ is set to be 0.5 and 1.0 for Scene 2, 0.5 and 1.5 for Scene 3; the result of Scene 1 with same crown ρ of 0.5 is illustrated as a reference to show the influence of the between-crown ρ .

Fig. 5(b)] are similar; thus, the results of Scene 2 are shown as an example.

B. LAI Retrieval of Realistic Discontinuous Canopies

The structure is much more complicated for the realistic trees than the abstract trees in two aspects: 1) clumping between leaves in the crown volume exists in the realistic canopies; 2) the ρ in the crown is heterogeneous. As a result, the Clumping Indices (1 indicates the vegetation in the footprint is homogeneous, and the smaller this value, the more severe the clumping effect is) are 0.74 and 0.59 for *Citrus* and *Oak*, respectively. The vertical ρ profiles are shown in Fig. 7(a) for *Citrus* and Fig. 7(b) for *Oak*.

In the nine realistic discontinuous canopies, LAI_PATH performs the best of the three methods (Fig. 7); it has the smallest error (2.3–19.9%) compared with LAI_e (47.7–68.2%) and LAI_{e_fcover} (26.3–40.9%). Specifically, taking scenes (scene 1-1, 2-1, and 3-1) with trees randomly located in the footprint

as examples, $\Delta_{\text{LAI_PATH}}$ are -11.4% , -2.3% , and -13.6% , respectively, for the pure *Citrus*, pure *Oak*, and mixed *Citrus* and *Oak* canopy. However, if just the between-crown clumping was corrected, $\Delta_{\text{LAI}_{e_fcover}}$ are -26.5% , -40.9% , and -38.0% , respectively. Fig. 8 shows the intermediate results of LAI_PATH, which include: the original waveform and the modified waveform of the canopy (a), the modified waveform and the actual vertical leaf area from DART (b), and the relative path length distributions estimated from the modified waveform (c).

Taking scenes (scene 1-1, 2-1, and 3-1) with trees randomly located in the footprint as examples, Fig. 8 shows that the original waveforms of the canopy are pretty different from the reference true vertical leaf areas (within every layer with a 0.15 m height), which approximately reflect the vertical profile of the canopy. However, after correction of the occlusion, it shows that the return signal of the lower canopy is enhanced significantly compared to the original waveform; the shape of the modified waveform is close to that of the vertical true leaf area. The

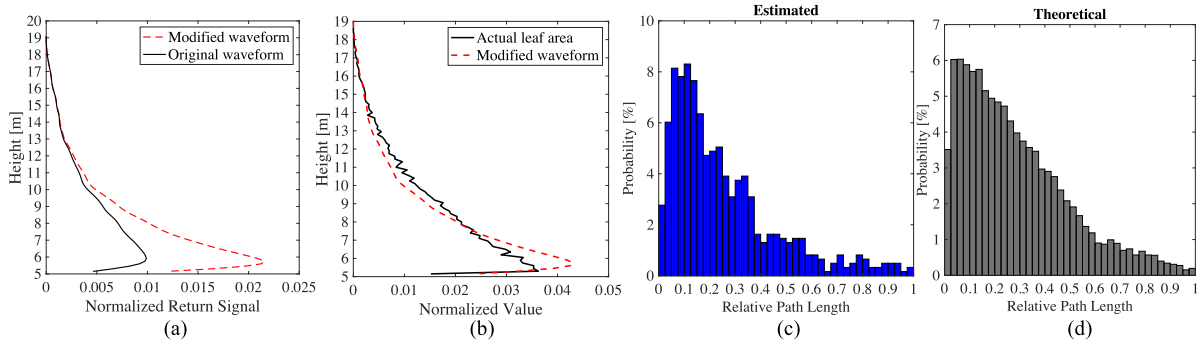


Fig. 6. Results of the discontinuous conical canopies [Scene 2 in Fig. 5(b)]: (a) the modified and the original waveform of the canopy, (b) the comparison of the modified waveform and the normalized true leaf area from DART, and (c) and (d) are the estimated relative path length distribution from the modified waveform and the calculated distribution by the ray tracing of the three-dimensional scenes.

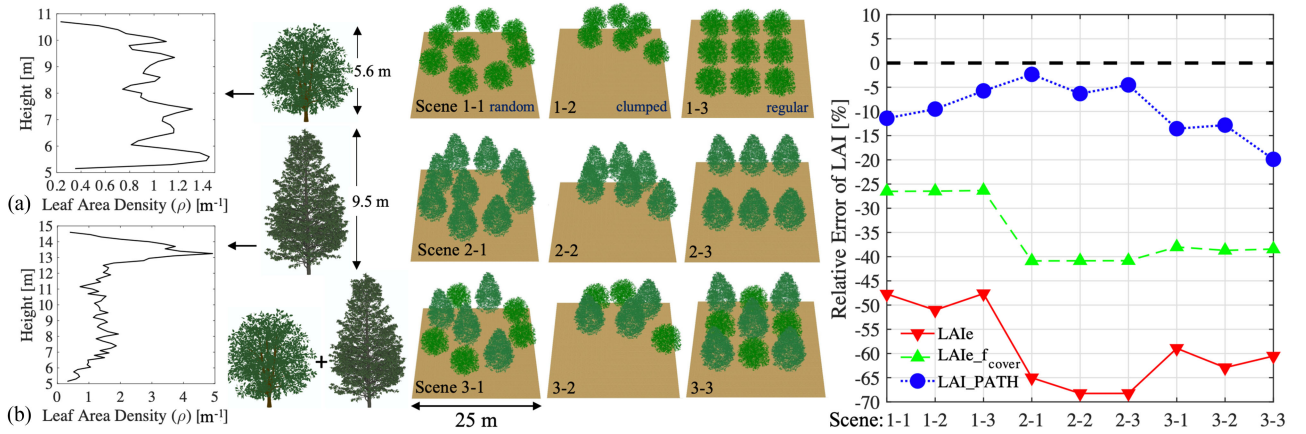


Fig. 7. Geometrical scenes and the relative errors of LAI from directly applying Beer's law (LAI_e), correcting the between-crown clumping ($\text{LAI}_{e_{f_{\text{cover}}}}$), and correcting both the between-crown and the within-crown clumping (LAI_{PATH}) for realistic discontinuous *Citrus*, *Oak* canopies, and the hybrid *Citrus* and *Oak* canopies without including the branches.

occlusion correction method seems effective when combined with the results in Fig. 8 and abstract spherical and conical canopies in Figs. 4 and 6.

C. LAI Retrieval of GLAS Footprints

There was no true LAI from the manual measurement of the leaves to validate the method. We used TRAC-measured LAI as a reference, even though it cannot represent the real LAI. A 21–33% underestimation of the gap size distribution method, which TRAC uses, was found in previous studies of ground-based indirect LAI measurements [20], [22], [58] because it cannot tackle the nonrandomness within the canopy enough. The gap size distribution method [15], [19] largely eliminates the large gaps that cannot appear in randomly distributed leaves; thus, it is essentially similar in principle with the method $\text{LAI}_{e_{f_{\text{cover}}}}$. It explains why $\text{LAI}_{e_{f_{\text{cover}}}}$ is close to TRAC measured LAI ($R^2 = 0.73$, $\text{RMSE} = 0.68$). Fig. 9 shows that the retrieved values of LAI_{PATH} are larger than the TRAC-measured LAIs for the studied plots ($R^2 = 0.74$, $\text{RMSE} = 1.18$) [Fig. 9(b)]. The possible reasons are as follows. 1) In addition to the between-crown clumping, the within-crown clumping is further corrected in method LAI_{PATH} , resulting in a larger LAI. Comparing Figs. 3 and 5, the within-crown clumping increases with crown ρ and crown length and is also dependent on the crown shape;

neglecting this clumping effect leads to an up to 46.7% underestimation in our simulated scenes. 2) Some sources of error are difficult to evaluate and might affect the performance of LAI_{PATH} , such as the error in f_{cover} estimation from passive optical imagery, and the error in gap probability estimation from the assumption that the ratio of reflectance of canopy and ground is 2.0 (as adopted in previous studies [10], [11]).

V. DISCUSSION

A. Occlusion Correction and its Role in Clumping Correction

The original waveform of the canopy is an apparent canopy profile, since objects further away from the LiDAR can be under-represented in the return signal due to occlusion by vegetation layers closer to the sensor. Thus, occlusion correction, which realizes a full utilization of the vertical structure information contained in LiDAR, is a vital procedure for clumping correction in our method. Only when the occlusion is corrected can one obtain the relative path length distribution, which characterizes the heterogeneity in the crown-covered regions, from the occlusion corrected waveform (assumed as the vertical canopy profile). Our basic idea of modifying the return signal is to establish a relationship between the observed return signals (affected by the occlusion of the upper canopy) and the corresponding signals as if the upper canopy did not exist. Thus, the return

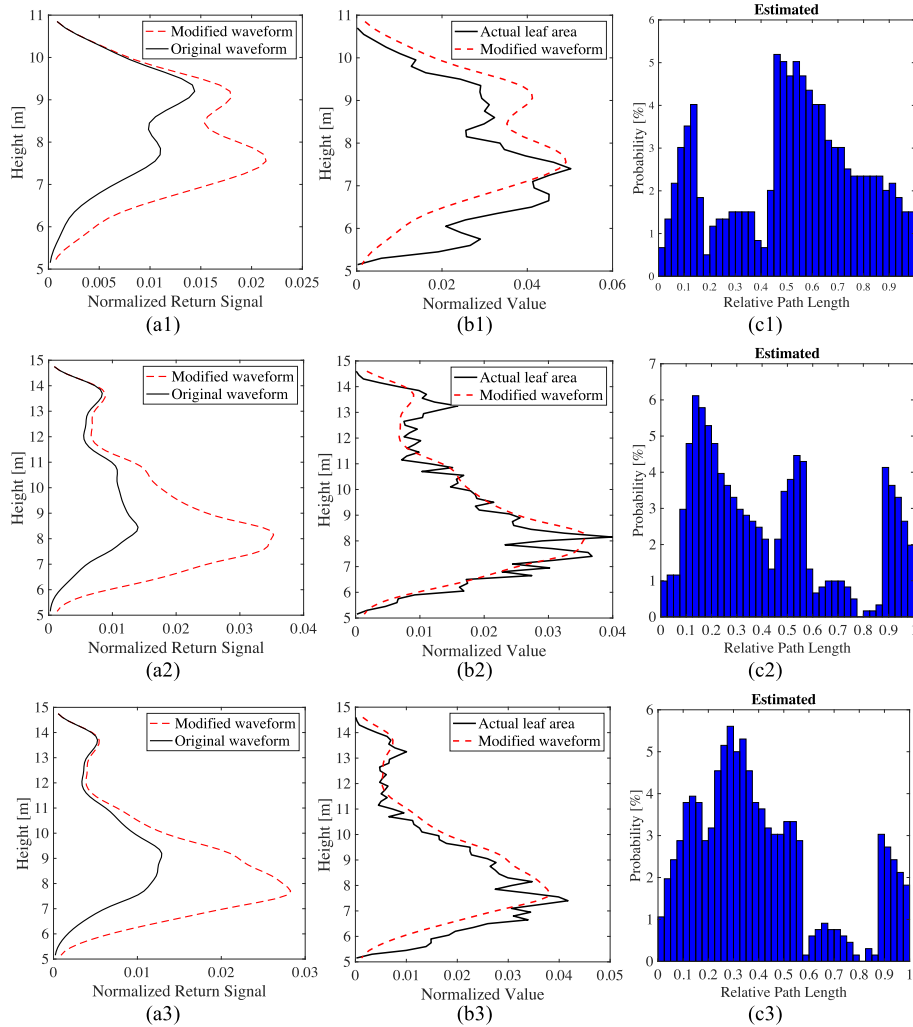


Fig. 8. Results of the realistic discontinuous *Citrus*, *Oak*, and hybrid *Citrus* and *Oak* canopies (corresponding to scene 1-1, 2-1, and 3-1 in Fig. 7): (a) the original and modified waveform for the canopy, (b) the comparison of the modified waveform and the normalized true vertical leaf area from DART, and (c) the estimated relative path length distribution from the modified waveform.

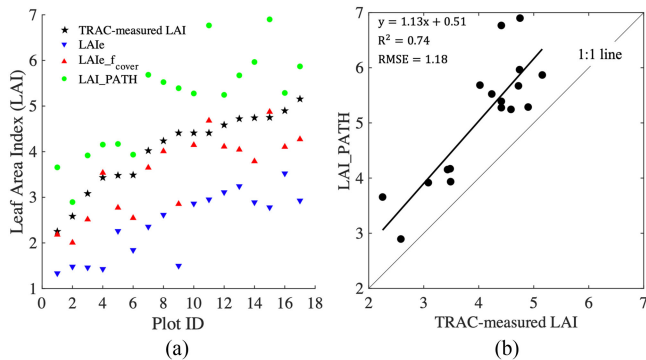


Fig. 9. Results of LAIs for GLAS footprints: (a) comparison of TRAC-measured LAI, GLAS-derived LAI_e (not correcting any clumping), $LAI_{e_f_cover}$ (correcting the between-crown clumping), and LAI_{PATH} (correcting both between-crown and within-crown clumping); (b) regression analysis of TRAC-measured LAI and GLAS derived LAI_{PATH} .

signal in the lower canopy is enhanced from the actual measured return signal, the crown coverage information, and the corresponding gap probability above the lower canopy, based on

three assumptions. 1) The reflectance of canopy components is vertically homogenous. 2) The canopy components are vertically independent of each other. 3) Despite the energy in the laser beam being a Gaussian distribution for both synthetic and GLAS data, it is assumed to be homogeneous across the beam footprint in the correction of the occlusion, and consequentially we ignore any bias caused by higher energy at the center of the beam [32]. Despite the potentially limited validity of the assumptions in the real world, our results show that the modified waveforms are closer in representing the vertical leaf area profiles from virtual scenes in comparison to applying no correction at all. This study focuses on the broadleaf tree species. In future work, the occlusion and clumping correction performance in coniferous species, where additional shoot-level clumping exists, needs to be evaluated via simulation.

B. Sensitivity of *PATH* Method

LAI_{PATH} is less sensitive to the increase of crown length and leaf area density (ρ) when compared with LAI_e and $LAI_{e_f_cover}$,

as Figs. 3 and 5 show. The derivation of LAI_PATH is based on the relationship between LAI, ρ , and path length. ($\rho \cdot l_{\max}$) is solved as a whole from (B1) and used in (B2) for LAI_PATH calculation. Thus, the ρ is assumed to be equal in crown-covered regions. It explains why errors of LAI_PATH increase [up to 19%, see Fig. 5(b)] if distinct ρ values with a three-fold difference are assigned to crowns compared with those when there is no heterogeneity of ρ between crowns [generally less than 10%, see Figs. 3 and 5(a)]. Besides, LAI_PATH is not that affected by vertical heterogeneity within-crown area compared with horizontal heterogeneity between-crowns in the footprint. As is noted from the relative error of LAI and the vertical ρ profile of the tree crowns of Scene 2 in Fig. 7, the error of LAI is less than 5% even though the ρ in the vertical direction is highly heterogeneous. It is because, essentially, only one ρ value is needed in the model inversion.

C. Future Research Perspectives

This work proposed a method of correcting the occlusion effect in vegetation waveforms and correcting the within-crown clumping in LAI retrieval from large-footprint full-waveform LiDAR. We tested its performance using synthetic data sets and GLAS data. Some aspects need further investigation.

- 1) A flat background is used in the generated synthetic data sets; however, many forests grow on mountains and undulating terrains, making it challenging to distinguish vegetation and ground response in the waveform [45], [59], [60]. The terrain will impact all the other biophysical variables (e.g., height, cover), not only the LAI retrieval method. How we could use this method in complex terrain, especially how to consider the impact of undulating terrain on the canopy profile and the identification of the canopy base height, needs to be studied.
- 2) Between-crown gap probability ($1 - f_{\text{cover}}$), vital for the between-crown clumping correction, cannot be obtained from large-footprint LiDAR due to the lack of information of the spatial distribution. We performed this study by assuming that the between-crown gap probability can be estimated from other data sources. To make a comparison of LAIs derived from our method (correcting both between-crown and within-crown clumping) with those from a previous study [11] (only correcting between-crown clumping), Landsat imagery was used in the estimation of f_{cover} . However, the combined utilization of data from different satellites limits the application of correcting the between-crown clumping indicated in [11]. The upcoming MOLI [9], which will conduct a simultaneous measurement using a LiDAR (25-m diameter footprint) and a high-resolution imager (green, red, and near-infrared band, with 5 m spatial resolution) on the same satellite, will be a better data source.
- 3) The occlusion correction method may be potentially helpful in the vertical LAI, ρ , or vertical foliage profile retrieval [13], [25], [61], and morphological forest traits like foliage height diversity (FHD) [62], [63], stand or stemwood volume [64], [65], and aboveground biomass [66] estimation

from the waveform; these are all closely related to the 3-D distribution of the canopy structure.

D. Possibilities of Multispectral LiDAR in Improving LAI Retrieval

The retrieved LAI from GLAS data is plant area index (PAI) due to the influence of the woody canopy components, which cannot be differentiated from green leaves and needles. GLAS was a multi-spectral LiDAR; however, the wavelength of 532 nm was explicitly designed for atmospheric research, and its lasers died quite early in the mission; thus, only the waveform of 1064 nm is used for LAI retrieval. If a future design of a multi-spectral LiDAR with properly selected wavelengths would be sensitive to the difference of reflectance property of leaves, branches, and the soil, the woody components, and the fraction of between-crown gaps can likely be better estimated. In addition, a multispectral LiDAR might help to better detect the ground in areas with topography [67], given a spectral gradient between canopy and ground. Morsdorf *et al.* [68] show in a virtual prototyping study that such a multi-spectral LiDAR with four wavelengths could effectively separate woody and leafy canopy volume and correct for occlusion to some amount.

VI. CONCLUSION

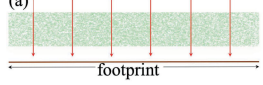
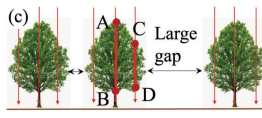
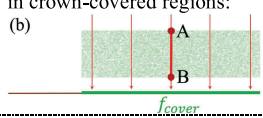
LAI is a crucial vegetation structure parameter. The demand for LAI retrieval from large-footprint full-waveform LiDAR increases with the increasingly available data. However, LAI retrieval needs to be improved due to the nonrandomness of foliage (i.e., clumping) within the footprint. New methods for compensating occlusion, and deriving relative path length distribution, which reflects the heterogeneity of canopy, from the occlusion corrected waveform, were presented. The clumping in the crown-covered regions, which has been ignored in previous methods, was corrected using the derived relative path length distribution, based on PATH theory. Results show that it is dependent on the crown shape and increases with crown leaf area density and crown length. Correcting the crown-level clumping improves the LAI underestimation problem significantly. The errors of our LAI retrieval method are generally around 10%, with the maximum error being below 20%; the maximum error may be as high as 69% and 47% for two current methods: one does not correct any clumping, the other corrects the clumping caused by between-crown gaps. Moreover, it is more stable in various scenes than the other methods.

Although these findings are mainly based on the synthetic data sets and more real LiDAR and field measurements need to be used to confirm them, our approach manifests a possible pathway to improve the LAI retrieval from large-footprint full-waveform LiDAR data.

APPENDIX

A. Current Physically-Based LAI Retrieval Methods From Spaceborne LiDAR

TABLE III
CURRENT TYPICAL PHYSICALLY-BASED MODELS FOR LAI RETRIEVAL FROM SPACEBORNE FULL-WAVEFORM LiDAR

Algorithm	Main formula	Assumption	Real forest
Beer's law [69], [70]	$P_{footprint}(\theta) = e^{-\frac{G(\theta) \cdot LAI_e}{\cos \theta}} \quad (A1)$ $LAI_e = -\frac{1}{G(\theta)} \cdot \ln(P_{footprint}(\theta)) \quad (A2)$	Homogeneity assumption in the entire footprint: (a) 	(c) 
Correcting between-crown clumping [11]	$P_{crown} = \frac{P_{footprint} - (1 - f_{cover})}{f_{cover}} \quad (A3)$ $LAI_{e, f_{cover}} = f_{cover} \cdot LAI_{crown}$ $= f_{cover} \cdot \left[-\frac{1}{G} \cdot \ln(P_{crown}) \right] \quad (A4)$	Homogeneity assumption in crown-covered regions: (b) 	↓ Observing direction AB , CD : Path length (<i>l</i>)

In (A1), $P_{footprint}(\theta)$ denotes the gap probability of the footprint in the viewing zenith angle θ ; $G(\theta)$ represents the mean leaf projection coefficient perpendicular to the observing direction, spherical leaf angle distribution is assumed in this work with a constant 0.5 for $G(\theta)$. θ is assumed to be 0° for spaceborne LiDAR, and we drop $\cos \theta$ in (A2), and θ in (A3) and (A4).
In (A3) and (A4), P_{crown} denotes the gap probability in the crown-covered region; f_{cover} is the fractional crown coverage within the footprint and is estimated from the Landsat imagery based on the dimidiate pixel model [71] in [11]. $(1 - f_{cover})$ means the between-crown gap probability. LAI_{crown} denotes the retrieved LAI of the crown-covered region.

B. Path Length Distribution Method

In the PATH, LAI_PATH can be retrieved by correcting both the between-crown and within-crown clumping as follows:

$$P_{crown} = \int_0^1 e^{-G \cdot (\rho \cdot l_{max}) \cdot l_r} \cdot p(l_r) d(l_r) \quad (B1)$$

$$LAI_{PATH} = f_{cover} \cdot \int_0^1 (\rho \cdot l_{max}) \cdot l_r \cdot p(l_r) d(l_r) \quad (B2)$$

where ρ is the leaf area density, l_r is the relative path length by normalizing the path lengths (l) to 1 concerning the maximum path length (l_{max}) ($l_r = l/l_{max}$), and $p(l_r)$ is the relative path length distribution which can characterize the heterogeneity in the crown, $\int_0^1 p(l_r) d(l_r) = 1$. With known P_{crown} , f_{cover} , $p(l_r)$, and G , the $(\rho \cdot l_{max})$ can be solved from (B1), then the LAI_PATH can be calculated using (B2). The within-crown clumping correction in LAI retrieval can be realized with known gap probability and $p(l_r)$.

ACKNOWLEDGMENT

The authors would like to thank the DART team in the data simulation. The authors thank the anonymous reviewers for their thoughtful and constructive reviews that helped us significantly improve the quality of the manuscript.

REFERENCES

- [1] S. C. Stark *et al.*, "Amazon forest carbon dynamics predicted by profiles of canopy leaf area and light environment," *Ecol. Lett.*, vol. 15, no. 12, pp. 1406–1414, Dec. 2012.
- [2] G. Yan *et al.*, "Review of indirect optical measurements of leaf area index: Recent advances, challenges, and perspectives," *Agricultural Forest Meteorol.*, vol. 265, pp. 390–411, 2019.
- [3] G. P. Asner, J. M. O. Scurlock, and J. A. Hicke, "Global synthesis of leaf area index observations: Implications for ecological and remote sensing studies," *Glob. Ecol. Biogeogr.*, vol. 12, no. 3, pp. 191–205, Apr. 2003.
- [4] R. O. Dubayah *et al.*, "The global ecosystem dynamics investigation: High-resolution laser ranging of the earth's forests and topography," *Sci. Remote Sens.*, vol. 1, 2020, Art. no. 100002.
- [5] W. Yang *et al.*, "MODIS leaf area index products: From validation to algorithm improvement," *IEEE Trans. Geosci. Remote Sens.*, vol. 44, no. 7, pp. 1885–1896, Jul. 2006.
- [6] J. B. Drake *et al.*, "Estimation of tropical forest structural characteristics, using large-footprint LiDAR," *Remote Sens. Environ.*, vol. 79, no. 2/3, pp. 305–319, 2002.
- [7] R. S. Afzal *et al.*, "The geoscience laser altimeter system (GLAS) laser transmitter," *IEEE J. Sel. Top. Quantum Electron.*, vol. 13, no. 3, pp. 511–535, May/June. 2007.
- [8] S. Hancock *et al.*, "The GEDI simulator: A large-footprint waveform LiDAR simulator for calibration and validation of spaceborne missions," *Earth Space Sci.*, vol. 6, no. 2, pp. 294–310, 2019.
- [9] D. Sakaizawa, R. Mitsuahahi, J. Murooka, T. Imai, T. Kimura, and K. Asai, "Current status of the ISS-vegetation LiDAR Mission-MOLI," in *Proc. Int. Geosci. Remote Sens. Symp.*, 2018, pp. 1861–1864.
- [10] S. Luo, C. Wang, G. Li, and X. Xi, "Retrieving leaf area index using ICESat/GLAS full-waveform data," *Remote Sens. Lett.*, vol. 4, no. 8, pp. 745–753, 2013.
- [11] X. Yang, C. Wang, F. Pan, S. Nie, X. Xi, and S. Luo, "Retrieving leaf area index in discontinuous forest using ICESat/GLAS full-waveform data based on gap fraction model," *ISPRS J. Photogramm. Remote Sens.*, vol. 148, pp. 54–62, 2019.
- [12] Beer, "Bestimmung der absorption des rothen lichts in farbigen flüssigkeiten," *Ann. Phys.*, vol. 162, no. 5, pp. 78–88, 1852.
- [13] H. Tang *et al.*, "Retrieval of vertical LAI profiles over tropical rain forests using waveform LiDAR at La Selva, Costa Rica," *Remote Sens. Environ.*, vol. 124, pp. 242–250, Sep. 2012.
- [14] H. Tang and J. Armston, "Algorithm theoretical basis document (ATBD) for GEDI L2B footprint canopy cover and vertical profile metrics," Goddard Sp. Flight Cent. Greenbelt, MD, USA, Tech. Rep., 2019. [Online]. Available: https://lpdaac.usgs.gov/documents/588/GEDI_FCCVPM_ATBD_v1.0.pdf
- [15] J. M. Chen and J. Cihlar, "Quantifying the effect of canopy architecture on optical measurements of leaf area index using two gap size analysis methods," *IEEE Trans. Geosci. Remote Sens.*, vol. 33, no. 3, pp. 777–787, May 1995.
- [16] P. Stenberg, "Correcting LAI-2000 estimates for the clumping of needles in shoots of conifers," *Agricultural Forest Meteorol.*, vol. 79, no. 1/2, pp. 1–8, Mar. 1996.
- [17] M. Weiss, F. Baret, G. J. Smith, I. Jonckheere, and P. Coppin, "Review of methods for in situ leaf area index (LAI) determination," *Agricultural Forest Meteorol.*, vol. 121, no. 1/2, pp. 37–53, Jan. 2004.
- [18] A. Lang, "Estimation of leaf area index from transmission of direct sunlight in discontinuous canopies," *Agricultural Forest Meteorol.*, vol. 37, no. 3, pp. 229–243, Aug. 1986.

- [19] S. Leblanc, J. Chen, and M. Kwong, "Tracing radiation and architecture of canopies. TRAC manual. Version 2.1.3," Nat. Resour. Canada, Canada Cent., 2002.
- [20] S. G. Leblanc, J. M. Chen, R. Fernandes, D. W. Deering, and A. Conley, "Methodology comparison for canopy structure parameters extraction from digital hemispherical photography in boreal forests," *Agricultural Forest Meteorol.*, vol. 129, no. 3/4, pp. 187–207, Apr. 2005.
- [21] R. Hu *et al.*, "Using airborne laser scanner and path length distribution model to quantify clumping effect and estimate leaf area index," *IEEE Trans. Geosci. Remote Sens.*, vol. 56, no. 6, pp. 3196–3209, Jun. 2018.
- [22] R. Hu, G. Yan, X. Mu, and J. Luo, "Indirect measurement of leaf area index on the basis of path length distribution," *Remote Sens. Environ.*, vol. 155, pp. 239–247, Dec. 2014.
- [23] T. Adams, P. Beets, and C. Parrish, "Extracting more data from LiDAR in forested areas by analyzing waveform shape," *Remote Sens.*, vol. 4, no. 3, pp. 682–702, 2012.
- [24] F. Morsdorf, B. Kötz, E. Meier, K. I. Itten, and B. Allgöwer, "Estimation of LAI and fractional cover from small footprint airborne laser scanning data based on gap fraction," *Remote Sens. Environ.*, vol. 104, no. 1, pp. 50–61, 2006.
- [25] W. Ni-Meister, D. L. B. Jupp, and R. Dubayah, "Modeling LiDAR waveforms in heterogeneous and discrete canopies," *IEEE Trans. Geosci. Remote Sens.*, vol. 39, no. 9, pp. 1943–1958, Sep. 2001.
- [26] T. Adams, P. Beets, and C. Parrish, "Another dimension from LiDAR—Obtaining foliage density from full waveform data," *Cent. Coast. Ocean Mapp.*, vol. 2011, 2011, Art. no. 12.
- [27] M. Béland, D. D. Baldocchi, J. L. Widlowski, R. A. Fournier, and M. M. Verstraete, "On seeing the wood from the leaves and the role of voxel size in determining leaf area distribution of forests with terrestrial LiDAR," *Agricultural Forest Meteorol.*, vol. 184, pp. 82–97, 2014.
- [28] J. Shao *et al.*, "Single scanner BLS system for forest plot mapping," *IEEE Trans. Geosci. Remote Sens.*, vol. 59, no. 2, pp. 1675–1685, Feb. 2020.
- [29] L. Li *et al.*, "An iterative-mode scan design of terrestrial laser scanning in forests for minimizing occlusion effects," *IEEE Trans. Geosci. Remote Sens.*, vol. 59, no. 4, pp. 3547–3566, Apr. 2021.
- [30] K. Cawse-Nicholson, J. Van Aardt, P. Romanczyk, D. Kelbe, K. Krause, and T. Kampe, "A study of energy attenuation due to forest canopy in small footprint waveform LiDAR signals," in *Proc. Amer. Soc. Photogrammetry Remote Sens. Annu. Conf.*, 2013, pp. 85–92.
- [31] K. Richter, R. Blaskow, N. Stelling, and H. G. Maas, "Reference value provision schemes for attenuation correction of full-waveform airborne laser scanner data," *ISPRS Ann. Photogramm. Remote Sens. Spat. Inf. Sci.*, vol. 2, no. 3W5, pp. 65–72, 2015.
- [32] I. Korpela, A. Hovi, and F. Morsdorf, "Understorey trees in airborne LiDAR data—Selective mapping due to transmission losses and echo-triggering mechanisms," *Remote Sens. Environ.*, vol. 119, pp. 92–104, Apr. 2012.
- [33] E. Lindberg, K. Olofsson, J. Holmgren, and H. Olsson, "Estimation of 3-D vegetation structure from waveform and discrete return airborne laser scanning data," *Remote Sens. Environ.*, vol. 118, pp. 151–161, Mar. 2012.
- [34] K. Richter, N. Stelling, and H.-G. Maas, "Attenuation correction of full-waveform airborne laser scanner data for improving the quality of volumetric forest reconstructions by simplified waveform history analysis," in *Proc. Eur. Remote Sens., New Opportunities Sci. Pract.*, 2014, pp. 16–20.
- [35] B. Bailey, M. Ponce de León, and E. S. Krayenhoff, "One-dimensional models of radiation transfer in heterogeneous canopies: A review, re-evaluation, and improved model," *Geoscientific Model Develop. Discuss.*, vol. 13, pp. 4789–4808, 2020.
- [36] J. Qi *et al.*, "LESS: Large-scale remote sensing data and image simulation framework over heterogeneous 3-D scenes," *Remote Sens. Environ.*, vol. 221, pp. 695–706, Feb. 2019.
- [37] P. Lewis, "Three-dimensional plant modelling for remote sensing simulation studies using the botanical plant modelling system," *Agronomie*, vol. 19, no. 3/4, pp. 185–210, 1999.
- [38] J.-P. Gastellu-Etchegorry *et al.*, "Simulation of satellite, airborne and terrestrial LiDAR with DART (I): Waveform simulation with quasi-Monte Carlo ray tracing," *Remote Sens. Environ.*, vol. 184, pp. 418–435, Oct. 2016.
- [39] P. R. J. North, J. A. B. Rosette, J. C. Suárez, and S. O. Los, "A Monte Carlo radiative transfer model of satellite waveform LiDAR," *Int. J. Remote Sens.*, vol. 31, no. 5, pp. 1343–1358, 2010.
- [40] A. C. Brenner *et al.*, "Derivation of range and range distributions from laser pulse waveform analysis for surface elevations, roughness, slope, and vegetation heights, algorithm theoretical basis document, v.4.1," Tech. Rep., 2003. [Online]. Available: http://www.csr.utexas.edu/glas/pdf/Atbd_20031224.pdf
- [41] T. Yin, N. Lauret, and J. P. Gastellu-Etchegorry, "Simulation of satellite, airborne and terrestrial LiDAR with DART (II): ALS and TLS multi-pulse acquisitions, photon counting, and solar noise," *Remote Sens. Environ.*, vol. 184, pp. 454–468, 2016.
- [42] T. Yin, J. Qi, B. D. Cook, D. C. Morton, S. Wei, and J. P. Gastellu-Etchegorry, "Modeling small-footprint airborne LiDAR-derived estimates of gap probability and leaf area index," *Remote Sens.*, vol. 12, no. 1, 2020, Art. no. 4.
- [43] M. Béland, J.-L. Widlowski, R. A. Fournier, J.-F. Côté, and M. M. Verstraete, "Estimating leaf area distribution in Savanna trees from terrestrial LiDAR measurements," *Agricultural Forest Meteorol.*, vol. 151, no. 9, pp. 1252–1266, Sep. 2011.
- [44] G. Ligot, P. Balandier, B. Courbaud, and H. Claessens, "Forest radiative transfer models: Which approach for which application?," *Can. J. Forest Res.*, vol. 44, no. 5, pp. 391–403, 2014.
- [45] Y. Pang, M. Lefsky, G. Sun, and J. Ranson, "Impact of footprint diameter and off-Nadir pointing on the precision of canopy height estimates from spaceborne LiDAR," *Remote Sens. Environ.*, vol. 115, no. 11, pp. 2798–2809, 2011.
- [46] G. Zheng and L. M. Moskal, "Leaf orientation retrieval from terrestrial laser scanning (TLS) data," *IEEE Trans. Geosci. Remote Sens.*, vol. 50, no. 10, pp. 3970–3979, Oct. 2012.
- [47] G. Yan *et al.*, "Quantitative evaluation of leaf inclination angle distribution on leaf area index retrieval of coniferous canopies," *J. Remote Sens.*, vol. 2021, pp. 1–15, 2021.
- [48] W. Wagner, A. Ullrich, V. Ducic, T. Melzer, and N. Studnicka, "Gaussian decomposition and calibration of a novel small-footprint full-waveform digitizing airborne laser scanner," *ISPRS J. Photogramm. Remote Sens.*, vol. 60, no. 2, pp. 100–112, 2006.
- [49] I. Korpela, "Acquisition and evaluation of radiometrically comparable multi-footprint airborne LiDAR data for forest remote sensing," *Remote Sens. Environ.*, vol. 194, pp. 414–423, Jun. 2017.
- [50] W. Wagner, "Radiometric calibration of small-footprint full-waveform airborne laser scanner measurements: Basic physical concepts," *ISPRS J. Photogramm. Remote Sens.*, vol. 65, no. 6, pp. 505–513, 2010.
- [51] S. Y. Kotchenova, "Modeling LiDAR waveforms with time-dependent stochastic radiative transfer theory for remote estimations of forest structure," *J. Geophys. Res.*, vol. 108, no. D15, pp. 4484–4486, 2003.
- [52] G. Schaepman-Strub, M. E. Schaepman, T. H. Painter, S. Dangel, and J. V. Martonchik, "Reflectance quantities in optical remote sensing—Definitions and case studies," *Remote Sens. Environ.*, vol. 103, no. 1, pp. 27–42, Jul. 2006.
- [53] M. A. Hofton, J. B. Minster, and J. B. Blair, "Decomposition of laser altimeter waveforms," *IEEE Trans. Geosci. Remote Sens.*, vol. 38, no. 4, pp. 1989–1996, Jul. 2000.
- [54] C. B. Markwardt, "Non-linear least squares fitting in IDL with MPFIT," 2009, *arXiv: 0902.2850v1*.
- [55] J. Armston *et al.*, "Direct retrieval of canopy gap probability using airborne waveform LiDAR," *Remote Sens. Environ.*, vol. 134, pp. 24–38, Jul. 2013.
- [56] S. Garrigues, D. Allard, F. Baret, and M. Weiss, "Quantifying spatial heterogeneity at the landscape scale using Variogram models," *Remote Sens. Environ.*, vol. 103, no. 1, pp. 81–96, Jul. 2006.
- [57] G. Yan *et al.*, "Scale effect in indirect measurement of leaf area index," *IEEE Trans. Geosci. Remote Sens.*, vol. 54, no. 6, pp. 3475–3484, Jun. 2016.
- [58] C. J. Kucharik, J. M. Norman, and S. T. Gower, "Measurements of branch area and adjusting leaf area index indirect measurements," *Agricultural Forest Meteorol.*, vol. 91, no. 1/2, pp. 69–88, May 1998.
- [59] Y. Wang, W. Ni, G. Sun, H. Chi, Z. Zhang, and Z. Guo, "Slope-adaptive waveform metrics of large footprint lidar for estimation of forest aboveground biomass," *Remote Sens. Environ.*, vol. 224, pp. 386–400, 2019.
- [60] J. A. B. Rosette, P. R. J. North, J. C. Suárez, and S. O. Los, "Uncertainty within satellite LiDAR estimations of vegetation and topography," *Int. J. Remote Sens.*, vol. 31, no. 5, pp. 1325–1342, Mar. 2010.
- [61] H. Tang, R. Dubayah, M. Brolly, S. Ganguly, and G. Zhang, "Large-scale retrieval of leaf area index and vertical foliage profile from the spaceborne waveform LiDAR (GLAS/ICESat)," *Remote Sens. Environ.*, vol. 154, pp. 8–18, Nov. 2014.
- [62] F. D. Schneider *et al.*, "Mapping functional diversity from remotely sensed morphological and physiological forest traits," *Nature Commun.*, vol. 8, no. 1, Dec. 2017, Art. no. 1441, doi: [10.1038/s41467-017-01530-3](https://doi.org/10.1038/s41467-017-01530-3).
- [63] Z. Zheng *et al.*, "Mapping functional diversity using individual tree-based morphological and physiological traits in a subtropical forest," *Remote Sens. Environ.*, vol. 252, 2020, Art. no. 112170.

- [64] P. Watt and M. S. Watt, "Development of a National Model of Pinus Radiata stand volume from LiDAR metrics for New Zealand," *Int. J. Remote Sens.*, vol. 34, no. 16, pp. 5892–5904, Aug. 2013.
- [65] J. Rosette, P. North, and J. Suarez, "Stemwood volume estimates for a mixed temperate forest using satellite LiDAR," *J. Forest Plan.*, vol. 13, pp. 205–214, 2008.
- [66] J. Boudreau, R. F. Nelson, H. A. Margolis, A. Beaudoin, L. Guindon, and D. S. Kimes, "Regional aboveground forest biomass using airborne and spaceborne LiDAR in Québec," *Remote Sens. Environ.*, vol. 112, no. 10, pp. 3876–3890, Oct. 2008.
- [67] S. Hancock, P. Lewis, M. Foster, M. Disney, and J.-P. Muller, "Measuring forests with dual wavelength LiDAR: A simulation study over topography," *Agricultural Forest Meteorol.*, vol. 161, pp. 123–133, Aug. 2012.
- [68] F. Morsdorf, C. Nichol, T. Malthus, and I. H. Woodhouse, "Assessing forest structural and physiological information content of multi-spectral LiDAR waveforms by radiative transfer modelling," *Remote Sens. Environ.*, vol. 113, no. 10, pp. 2152–2163, 2009.
- [69] C. T. de Wit and C. T. de Wit, "Photosynthesis of leaf canopies," Wageningen Univ., Wageningen, The Netherlands, Tech. Rep. 663, 1965.
- [70] J. L. Monteith, "Light distribution and photosynthesis in field crops," *Ann. Botany*, vol. 29, no. 1, pp. 17–37, 1965.
- [71] G. Wang, G. Gertner, S. Fang, and A. B. Anderson, "Mapping vegetation cover change using geostatistical methods and bitemporal Landsat TM images," *IEEE Trans. Geosci. Remote Sens.*, vol. 42, no. 3, pp. 632–643, Mar. 2004.



Shiyu Cheng received the M.Sc. degree in mapping and geography information systems from Beijing Normal University, Beijing, China, in 2021.

Her research interests include leaf area index estimation, clumping effect correction, and terrestrial laser scanning.



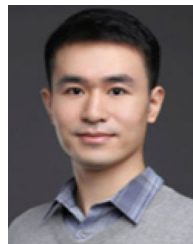
Xuebo Yang received the joint Ph.D. degree in mapping and geography information systems from the Aerospace Information Research Institute, Chinese Academy of Sciences, Beijing, China, and the College of Resources of Environment, University of the Chinese Academy of Sciences, Beijing, China.

Her research interests include LiDAR radiative transfer modeling, design of LiDAR sensors, and multifield applications of LiDAR data.



Hailan Jiang received the M.Sc. degree in mapping and geography information systems from Lanzhou University, Lanzhou, China, in 2015. She is currently working toward the Ph.D. degree in mapping and geography information systems with Beijing Normal University, Beijing, China.

Her research interests include the estimation of vegetation structure from laser scanning data.



Ronghai Hu received the Ph.D. degree in remote sensing from Beijing Normal University, Beijing, China, and ICube Laboratory, Centre National de la Recherche Scientifique (CNRS), University of Strasbourg, Strasbourg, France, in 2018.

His research interests include indirect measurement and airborne retrieval of leaf area index (LAI), remote sensing of vegetation, light detection and ranging (LiDAR), and scale effect on remote sensing.



Guangjian Yan (Senior Member, IEEE) received the Ph.D. degree in mapping and geography information systems from the Institute of Remote Sensing Applications, Chinese Academy of Sciences, Beijing, China, in 1999.

He is currently a Professor with the State Key Laboratory of Remote Sensing Science, Institute of Remote Sensing Science and Engineering, Faculty of Geographical Science, Beijing Normal University, Beijing, China. He has authored or coauthored more than 200 papers. His research interests are multi-

angular remote sensing, vegetation remote sensing, radiation budgets, and scale effects in remote sensing.



Linyuan Li (Associate Member, IEEE) received the Ph.D. degree in mapping and geography information systems from Beijing Normal University, Beijing, China, in 2020.

His research interests include unmanned aerial vehicle (UAV)-based remote sensing of vegetation, multiangular remote sensing, and light detection and ranging (LiDAR) data processing.



Yiyi Tong received the M.Sc. degree in mapping and geography information systems from Beijing Normal University, Beijing, China, in 2020.

Her research interests include the estimation of radiation budgets and the validation of remote sensing models in rugged terrains.



Xihan Mu received the Ph.D. degree in remote sensing from the School of Geography, Beijing Normal University, Beijing, China, in 2009.

He is currently an Associate Professor with the State Key Laboratory of Remote Sensing Science, Institute of Remote Sensing Science and Engineering, Faculty of Geographical Science, Beijing Normal University. His research interests include multiangular remote sensing, especially in the retrieval/measurement of vegetation structural parameters.



Donghui Xie received the Ph.D. degree in remote sensing and geographic information systems from Beijing Normal University, Beijing, China, in 2005.

She is currently an Associate Professor with the State Key Laboratory of Remote Sensing Science, Institute of Remote Sensing Science and Engineering, Faculty of Geographical Science, Beijing Normal University. Her research interests include canopy radiative transfer modeling, biophysical parameter retrieval of vegetation, and remote sensing data fusion.



Guoqing Zhou received the Ph.D. degree in photogrammetry and remote sensing from Wuhan University, Wuhan, China, in 1994.

He is currently a Professor with the Guangxi Key Laboratory for Spatial Information and Geomatics, Guilin University of Technology, Guilin, China. His research interests include photogrammetry and remote sensing, especially in remote sensing image processing and interpretation.



Wuming Zhang received the Ph.D. degree in materials science and engineering from Tsinghua University, Beijing, China, in 2004.

He is a Professor with the School of Geospatial Engineering and Science, Sun Yat-sen University, Zhuhai, China. His research interests include photogrammetry and remote sensing, especially light detection and ranging (LiDAR) point cloud processing, and applications.



Felix Morsdorf received the Ph.D. degree and *venia legendi* in geography, with a specialization in LiDAR remote sensing, from the University of Zurich, Zurich, Switzerland, in 2007 and 2021, respectively.

He is a Group Leader with the Department of Geography, University of Zurich. His group uses empirical and physical approaches to bridge the semantic gap between data and information in the context of laser scanning and vegetation structure.